Graphical Abstract:

Synthesis via sequential deposition of polydiallyldimethylammonium chloride (PDDA), delaminated-manganese oxide (MnO_2) and functionalized carbon nano-onions (ONCNOs) produces high-performance supercapacitor electrodes.
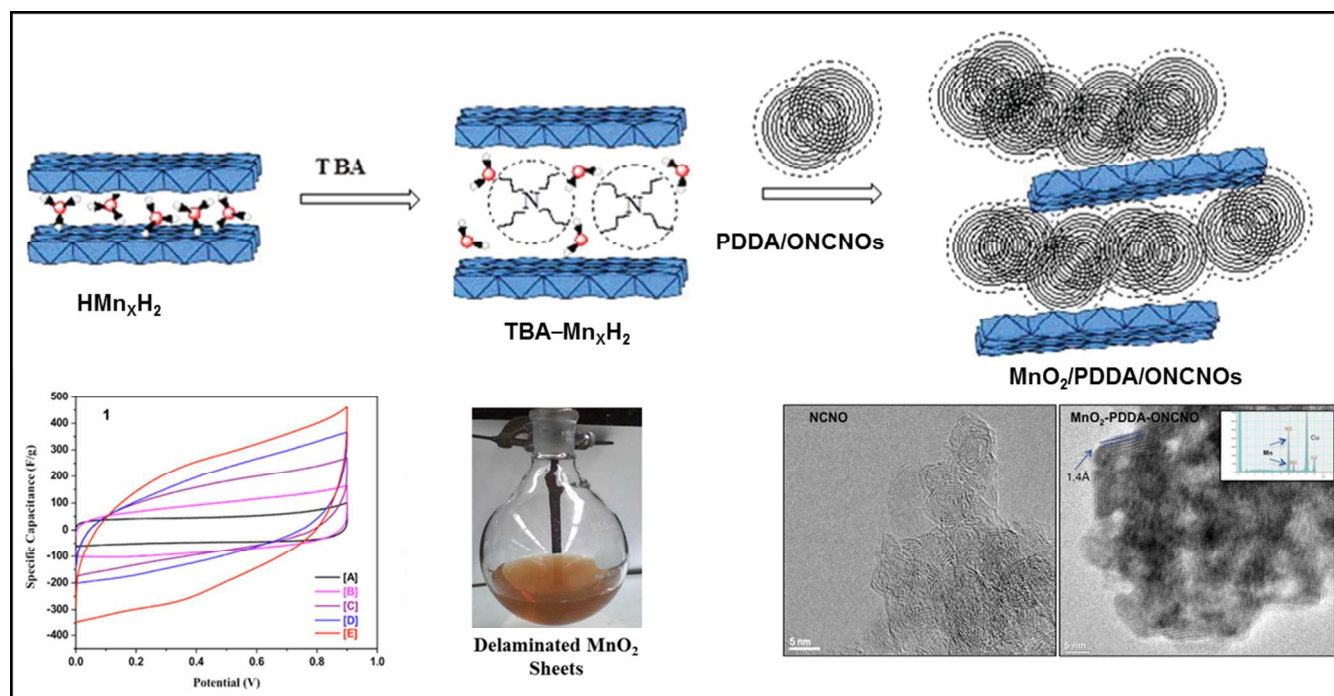
Ternary composites of delaminated-MnO₂/PDDA/functionalized-CNOs for high-capacity supercapacitor electrodes.

Rituraj Borgohain* [1, 3], John P. Selegue[1], Y.-T. Cheng[2]

[1]Department of Chemistry and [2]Department of Chemical and Materials Engineering, University of Kentucky, Lexington, Kentucky 40506, USA.

Abstract:

Composite materials are synthesized by combining chemically functionalized carbon nano-onions (ONCNOs), a polyelectrolyte (polydiallyldimethylammonium chloride, PDDA) and delaminated layered-manganese oxides (MnO₂). While carbon nano-onions are one of the least studied carbon allotropes to date, extensive research has been reported on various types of crystalline and amorphous MnO₂ to overcome their limitations for energy storage applications. We have developed a synergistically tuned synthesis of MnO₂-based composites with NCNOs via sequential chemical deposition technique to achieve high-capacity supercapacitor electrodes with long-term stability. Composite with 55 wt % MnO₂ on PDDA modified ONCNOs exhibits high-capacitance of 218.6 F•g^{-1} in a symmetric two–electrode cell containing aqueous electrolyte (1.0 M Na₂SO₄) with a high-energy density of 6.14 Wh•kg^{-1}. Analytical techniques, such as high-resolution transmission electron microscopy, x-ray diffraction, atomic force microscopy, thermogravimetric analysis, and electrochemical measurements (cyclic voltammetry, galvanostatic charge-discharge, impedance), are employed to fully characterize the synthesized materials and to understand their electrochemical behavior. Emphasis is also given to understand the phenomenon that promotes higher capacitance and long-term stability of such composites based on MnO₂ redox chemistry.

Keywords: Carbon nano-onions, Supercapacitor, Manganese oxide, Composite

*Corresponding author's present address: [3]EORI, School of Energy Dept. # 4068, 1000 E.

University Ave., University of Wyoming, Laramie, Wyoming 82071, USA

 Email: rborgoha@uwyo.edu. (307) 7662735, (307) 766-2737 (fax).

2

1. Introduction:

The studies and applications of supercapacitor gained pace after the patent filed by General Electric in 1957 on porous carbon electrodes with exceptional charge storage.[1] With increase in demand for high-power and high-energy devices, requirements for advance energy storage systems are escalating. Therefore research on supercapacitors, which serve as a bridge between high-energy-density batteries and high-power-density electrolytic capacitors, have attracted much attention. Supercapacitors store energy at the interface of electrode and electrolyte. To enhance the energy density of supercapacitor materials tremendous efforts have been given by adding transition metal oxides on high surface area carbonaceous materials. The redox properties of transition metal oxides produce pseudocapacitance (charge storage via Faradic reactions on the surface and the bulk of the material), enabling large capacity and high-energy density with some sacrifice in the high-power density behavior of traditional supercapacitors.

Manganese oxide is a popular choice for its redox behavior that can be utilized to enhance energy storage in supercapacitor electrodes. Low-cost, environment friendly and reasonably high specific capacitance of MnO_2-based electrodes gain much research attentions from the scientific community.[2, 3] However, poor electrical conductivity and irreversible redox chemistry of MnO_2 beyond a narrow potential range in aqueous electrolyte raise questions about its commercial value. To mitigate the poor electrical conductivity of MnO_2 various types of novel conductive nano carbon sources such as carbon nanotube (CNT),[4, 5] carbon nanofoams,[6] carbon nanofiber,[7] carbon nanowall,[8] graphene,[9, 10] and combination of carbon nanoparticles-polymer,[11] are add to the MnO_2 electrodes. Moreover, a thin layer of MnO_2 is coated both chemically[12] and

3

electrochemically[13] on supported materials to reduce the ion diffusion path length, which enhances the overall conductivity and reduces the equivalent series resistance (ESR) to achieve high power density. Specific capacitance of 100-410 $F \cdot g^{-1}$ in aqueous electrolyte were reported in recent literatures on MnO_2-carbon composite electrodes.[8, 14] However, these reported values depend on various factors such as cell type, scan rate, active mass, potential window and electrolyte. Among other conductive carbon sources, carbon nano-onions (CNOs) are a special type that caught attention to researcher for variety of applications especially for energy storage.[15-18] As-produced CNOs have high surface area, good conductivity and appropriate mesoporosity to serve as electrode materials for supercapacitor applications. In particular, nanodiamond-derived carbon nano-onions (NCNOs) with an average diameter of ~5–7 nm can be prepared in bulk quantities with homogeneous size distribution and high purity. NCNOs have BET surface area of ~520 $m^2 \cdot g^{-1}$, electrical conductivity of 4 $S.cm^{-1}$ and appropriate mesoporosity (2-50 nm). [16] Although the study of NCNOs for supercapacitors is not extensively documented, recent studies revealed their competitiveness with CNTs and other well-studied carbon allotropes.[16, 19-21] Moreover, unlike other amorphous carbon sources, the sp^2–C network of CNOs can enhance the charge transfer processes in metal oxide impregnated carbon supercapacitors. Therefore, CNOs are a very competitive carbon support, which can be prepared easily and cost-effectively in bulk quantities, for high-performance composite supercapacitor electrodes.

In this manuscript we focus on the synthesis of ternary composite electrodes of NCNOs, PDDA and delaminated-MnO_2 by a sequential chemical deposition technique. We synthesized MnO_2/PDDA/ONCNOs nanocomposites to achieve positive synergistic

4

effects based on opposite charge of each alternate layer and to utilize the high surface area of NCNOs for maximum utilization of the manganese oxide redox active sites for Faradic reactions. Electrochemical behaviors of the composites were studied in terms of performance and long-term stability in aqueous electrolyte for supercapacitor applications. MnO_2 (55 wt %)/PDDA/ONCNOs composites show enhanced specific capacitance up to 218.6 $F•g^{-1}$ in aqueous electrolyte in a symmetric two-electrode cell with a high-energy density of 6.14 $Wh•Kg^{-1}$.

2. Experimental

2.1 Materials:

Concentrated sulfuric acid and nitric acid (J. T. Baker), potassium permanganate ($KMnO_4$), polydiallyldimethylammonium chloride (PDDA), sodium sulfate (Na_2SO_4), and tetrabutylammonium hydroxide (TBA) (Sigma-Aldrich), and poly(vinylidene fluoride) (PVdF) (Alfa Aesar) were obtained commercially and used without purification.

2.2 Synthesis of NCNOs

Carbon nano-onions (5−7 nm diameter) were synthesized by the method we reported earlier.[16] In brief, nanodiamonds (Dynalene NB50) were annealed at 1650 °C for 1.0 h under helium in a graphitization furnace, which was followed by further annealing at 400 °C for 4 h under air to remove any amorphous carbon.

2.3 Synthesis of functionalized NCNOs (ONCNOs)

ONCNOs were synthesised according to our previously reported method via controlled oxidation of CNOs under acidic conditions.[16] In brief, NCNOs (0.050 g) were dispersed in concentrated H_2SO_4 (35 mL) by stirring for 24 h at room temperature. A

mixture of H_2SO_4 (15 mL) and HNO_3 (70%, 22 mL) was slowly added to the NCNO dispersion with continuous stirring and the resultant mixture was heated to 80−82 °C in an oil bath with continuous stirring for another 0.5 h. The dispersion was centrifuged and water was decanted. The material was resuspended in distilled water and subsequently collected by filtration on a 0.2 **µ**m microporous membrane, and finally vacuum-dried overnight at 45 °C.

2.4 Synthesis of PDDA/ONCNO

ONCNOs (0.120 g) were added to 200 mL deionized H_2O and stirred vigorously for 10 min, followed by horn sonication for another 5 min to obtain a well-dispersed solution. To this solution PDDA (0.2 mL) was added dropwise and stirring was continued at room temperature for 10 min. The resultant viscous reaction mixture was centrifuged and the product was separated out. The sample was washed several times (5×200 mL) with distilled water and filtered through a 0.2 micron membrane filter. The final product was dried under vacuum at 60 ºC overnight.

2.5 Synthesis of delaminated MnO_2

Thin sheets of delaminated MnO_2 were prepared via an ion-exchange method reported in the literature.[23,24] In brief, a 100 mL solution of ethanol (45 mL) and potassium hydroxide (16.8 g) was slowly added to the 100 mL solution of potassium permanganate (6.32 g) under vigorous stirring for 1 h. The precipitate obtained was aged at 80 ºC in an oven for 48 h. The resultant product was washed on filter paper with deionized water until the filtrate pH $<$ 9. The wet sample of K_xMnO_2 was proton-exchanged with 1-M HNO_3 at room temperature for 24 h followed by washing with

6

deionized water until the pH > 6 to ensure the removal of excess acids. The product was ion-exchanged with amines (TBA, 1:1 amine: Mn mole ratio) under room temperature stirring for 72 h. The resultant gel was washed with copious amount of deionized water and the wet sample was subsequently characterized by XRD. The delaminated MnO_2 layers form a yellow dispersion in water.

2.6 Synthesis of MnO₂/PDDA/ONCNOs composites

In a typical synthesis of the MnO_2/PDDA/ONCNOs composite, PDDA/ONCNOs (0.040 g) in distilled H_2O (150 mL) was horn-sonicated for 10 min using an ice bath. To the well-dispersed PDDA/ONCNOs solution, a calculated amount of delaminated MnO_2 dispersion was added and stirred at room temperature overnight followed by stirring at 70 ºC for 6 h. The resultant product was centrifuged, washed with water, and dried under vacuum at 60 ºC overnight.

3. Characterization

X-ray Diffraction (XRD) patterns of the samples were collected on a Bruker D8 Discover diffractometer using Cu-Kα radiation (40 kV, 40 mA). Samples were scanned over a 2θ range 2°−40° in a step-scan with 0.05°/step. JEOL 2010F field-emission transmission electron microscope (TEM) was used for the size and morphology study of the samples. Also, x-ray energy-dispersive spectrometer (EDS, Oxford) equipped with the JEOL 2010F was used for elemental identification. MikroMasch NSC-14 tips (150 kHz) were used for the topography characterization in the ac mode of the Agilent PicoPlus3000 environmental Atomic Force Microscopy (AFM). AFM images were processed using WSxM. A thin film of the material was prepared on a cleaned (boiled in

7

piranha solution (2:1 98% H_2SO_4/30% H_2O_2) at 125 °C for 15 min to remove organic contaminants, followed by washing with water and dry under vacuum) ultra-flat Si wafer (1x1cm^2). Zeta potentials measurements were done by using a zetasizer analyzer (Nano ZS, Malvern) by electrophoresis light scattering method. Samples (0.13 wt %) were dispersed in 10 mM NaCl solutions by ultrasonication for 30 mint and the zeta potential was measured at pH 7.

Electrochemical behavior of the composite electrodes were studied using cyclic voltammetry and galvanostatic cycling with a potentiostat (MPG2, BioLogic) and using electrochemical impedance spectroscopy (EIS) with an impedance analyzer (VMP3, BioLogic). A 5 wt % poly(vinylidene fluoride) (PVdF) was used as a binder with the active materials (0.2–0.25 mg) and a slurry was prepared with a few drops of N-Methylpyrrolidone to febricate a thin layer (~ 6μm) on the electrodes (gold plates, 9.5 mm diameter X 0.14 mm thickness), followed by drying under high-vacuum at 70 ºC for 24 h. The two electrodes in the symmetric Swagelok cell were separated by a microporous trilayer polypropylene membrane (Celgard 3501, 25 μm) soaked with 1.0 M Na_2SO_4. Cyclic voltammetry was measured at the scan rate of 5 mV/s in the voltage range of 0 to 0.9 V. Galvanostatic charge-discharge was carried out at a constant current density of 2.0 A/g in the voltage range 0–0.9 V. For EIS, the amplitude of the AC signal applied to the electrodes was 10 mV and the frequency was varied from 10 kHz to 10 mHz.

4. Results and Discussion:

Hydrous oxides of amorphous manganese oxides undergo reversible redox reactions by proton and/or cation exchange with the electrolyte, giving a large pseudocapacitance. In neutral electrolytic conditions hydrous MnO_2 undergos following chemical changes:[25]

$$MnO_x(H_2O)_y \rightleftharpoons MnO_{(x+\delta)}(H_2O)_{(y-\delta)} + 2\delta H^+ + 2\delta e^-$$
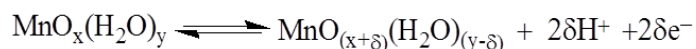
We have utilized the birnessite structure of layered K_xMnO_2 to prepare MnO_2 single sheets via an ion exchange method. The delaminated MnO_2 single sheets carry partial negative charges that are stabilized by TBA ions in solution. **Figure 1** depicts the sequential deposition approach to synthesize the MnO_2/PDDA/ONCNOs composites. Initially, carbon nano-onions are functionalized with polar carboxylic acid groups to increase their surface wettability.
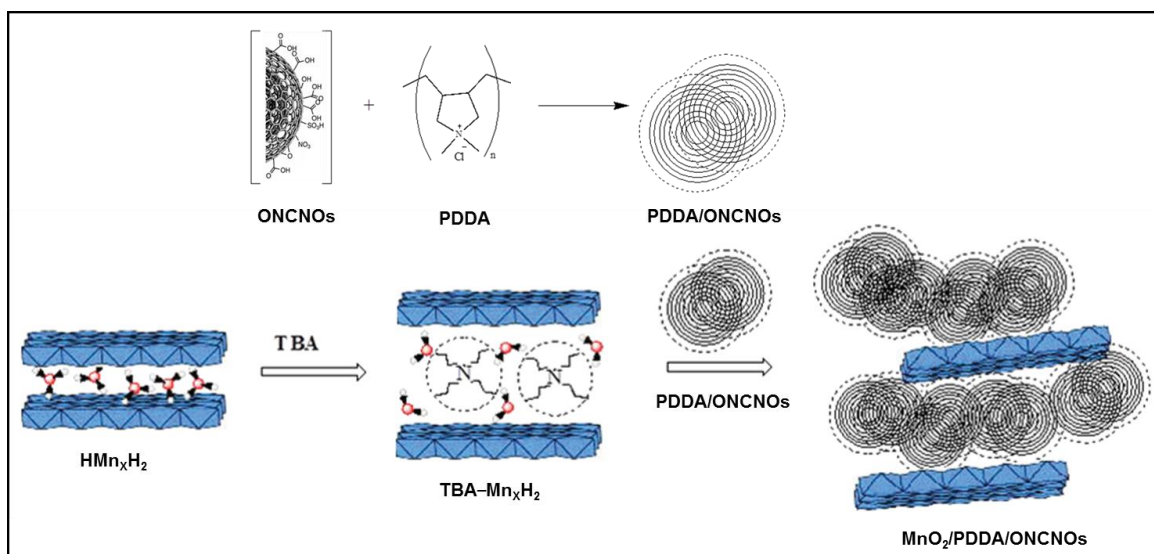
Figure 1. Step-by-step depiction of the synthesis of MnO_2-PDDA-ONCNO composites. (Cartoons are for schematic presentations only and not to scale).

For the aqueous electrolyte, hydrophilicity of the electrode facilitates access of the ions to the electrode/electrolyte interface, enhancing charge storage. Both NCNOs and chemically modified ONCNOs have good electrical conductivity, appropriate mesoporosity for ion transport, and high electrochemical and thermal stability.[16] After NCNOs are functionalized with acidic groups to form a negatively charged surface, a thin layer of positively charged PDDA molecules is coated on the surface. Zeta potential measurement of ONCNOs and PDDA/ONCNOs yielded the surface charge of $-$ 39.8 mV and $+$ 54.1 mV respectively at pH 7. The zeta potential changed from negative charge to positive charge when the cationic polyelectrolyte PDDA was self-assembled on the surface of ONCNOs. Strong electron accepting ability of the quartenary ammonium functional group of PDDA effectively binds to the uncharged surface of carbon nanoparticles and also adsorb onto negatively charged surfaces via electrostatic interactions.[26] The positively charged surface of PDDA/ONCNOs composite guides the negatively charged MnO_2 nano-sheets to attach to the surface. The final MnO_2/PDDA/ONCNOs composites, produced via sequential deposition, are formed to maximize the exposure of MnO_2 redox-active sites and also, to have a desiable synergistic effect of MnO_2 layers with the functionalized NCNOs for higher capacity and cycling stability.   The delaminated MnO_2 nano-sheets are examined by XRD analysis. After centrifugation (3500 rpm) of the MnO_2 dispersion, some of the materials are deposited at the bottom of the centrifugation tube, containing highly-separated MnO_2 nano-sheets, while the yellow supernatant solution contains single sheets of MnO_2. As

shown in **Fig. 2**, XRD of wet samples (before washing with H_2O) indicate highly-separated MnO_2 nano-sheets with an ordered structure while exfoliated MnO_2 sheets (after repeated washing with H_2O) produce broad diffraction peaks with low intensities.
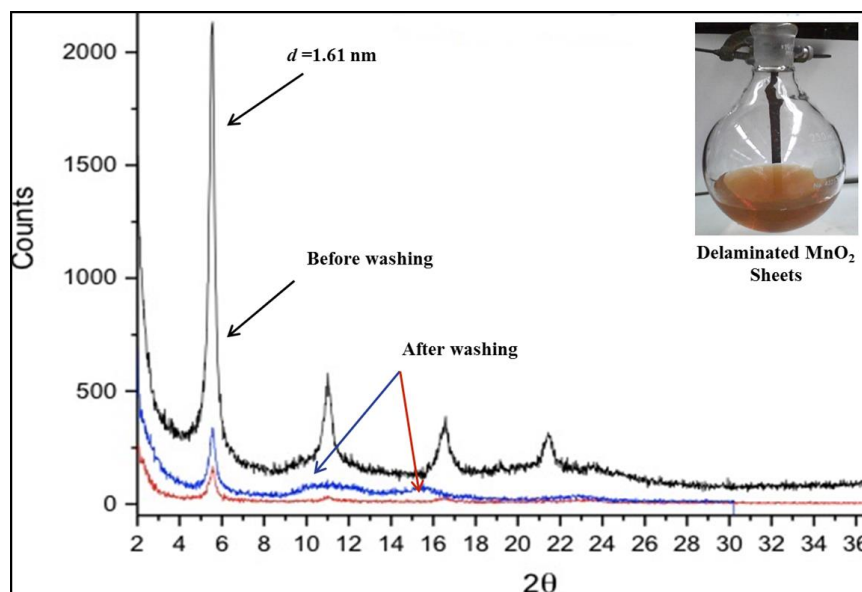
Figure 2. XRD of delaminated-MnO_2 wet precipitate before and after washing.

After repeated washing of highly-seperated MnO_2 layers delamination occurs due to the decrease in surface charge density of MnO_2 layers and the decrease in interlayer ion concentration. These observations are in agreement with other reported results. [22, 23]

For the PDDA/ONCNOs, it is important to control the thickness of the PDDA layer on ONCNO. A thicker polymer layer can prevent appropriate utilization of high surface area and electric conductivity of the carbon nano-onions, resulting in poor communication with the impregnated MnO_2 nano-sheets.

11
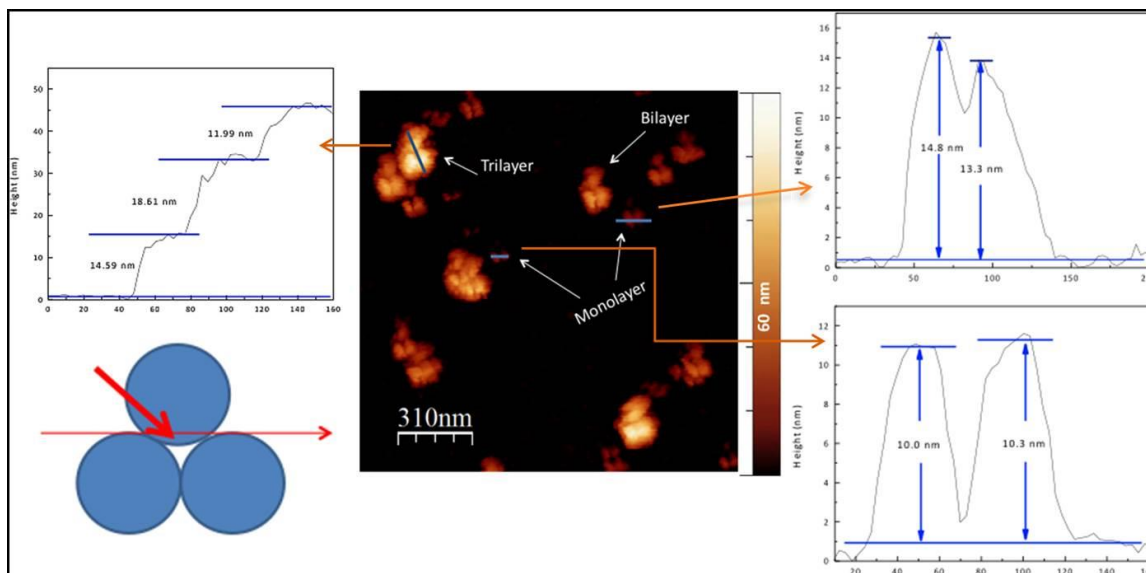
Figure 3. AFM analysis of PDDA/ONCNOs. Different spots are indicated along with their height profile measurements, and the cartoon shows a possible staking of nano-onion particles for multilayer spots.

AFM analysis on PDDA/ONCNOs is shown in **Fig. 3**. The height profile measurements from different spots comprising mono-, bi- and multilayers of PDDA/ONCNO materials indicate an average of ~3 nm thick PDDA layer, which is ~15 wt % of the PDDA/ONCNOs, homogeneously coated on ONCNOs (5–7 nm). The wt % of MnO_2 in the composites are determined from their residues obtained after thermogravimetric analysis at 800 ºC under air (**Fig. S1** in the supplimentary information). **Fig. 4** shows the HRTEM image of the MnO_2/PDDA/ONCNOs composite (55 wt % MnO_2). Both amorphous and semi-crystalline phases of the delaminated MnO_2 layers are observed. While the presence of the amorphous regions indicates a single layer of MnO_2 deposited on PDDA/ONCNOs, in the semi-crystalline phase a *d*-spacing of ~1.4

Å indicates re-aggregation of MnO_2 nanosheets. The re-aggregation of delaminated

MnO_2 layers upon drying is also reported by other groups.[23, 24]
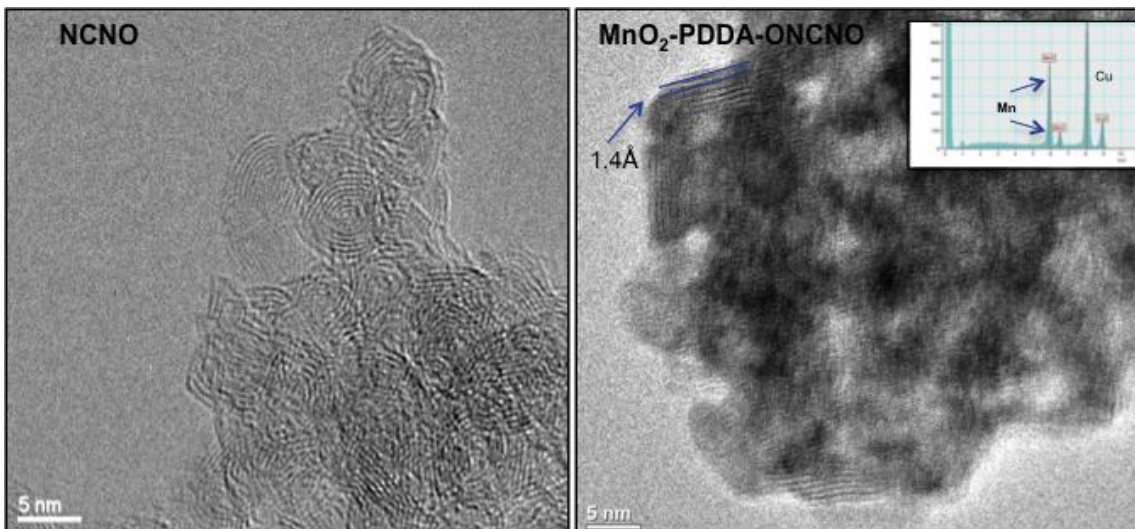
Figure 4. HRTEM images of NCNO vs. MnO_2/PDDA/ONCNOs composite. The

satellite image shows the EDX of the MnO_2/PDDA/ONCNOs composite.

The specific capacitance (C_{sp}) of the single electrode in the symmetric cell and

the maximum energy density (E_{max}) are determined by using the following equations:

$$C_{sp} = \frac{2C_{cell}}{m} = \frac{|I_a - I_c|}{m\left(\frac{dV}{dt}\right)} \quad (F.g^{-1})$$

$$E_{max} = \frac{C_{sp} V^2}{8(3.6)} \quad (Wh.kg^{-1})$$

where C_{cell} is the cell capacitance (F), m is the average mass (g) of the active

material of the single electrode, I_a and I_c (A) are the anodic and cathodic currents, $|I_a - I_c|$

is obtained by integrating the voltammogram and dividing by the voltage range, dV/dt is

the potential scan rate (V/s), and V is the cell potential.
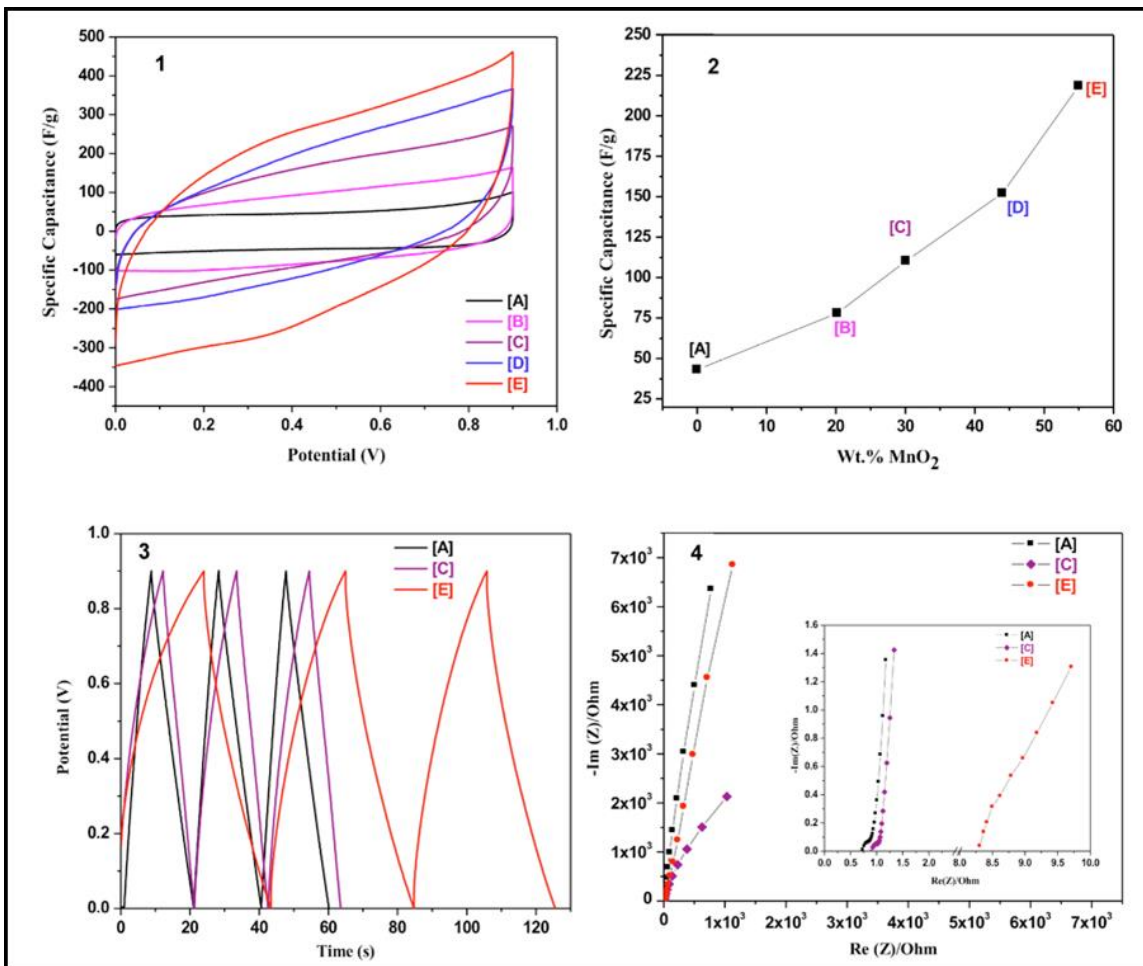
Figure 5. (**1**) Cyclic voltammetry (**2**) Plot of wt % MnO_2 vs. Specific capacitance

($F\bullet g^{-1}$) (**3**) Galvanostatic charge discharge (**4**) Impedance spectra of selected composites.

[A] PDDA/ONCNOs [B] MnO_2 (20.2 wt %)/PDDA/ONCNOs [C] MnO_2 (30.1 wt

%)/PDDA/ONCNOs [D] MnO_2 (44.0 wt %)/PDDA/ONCNOs [E] MnO_2 (55.0 wt

%)/PDDA/ONCNOs.

14

All the capacitance are obtained by using a two-electrode full cell. While three-electrode cells usually overestimate the capacitance, two-electrode configurations give good agreement with industrial cells. The CV of the PDDA/ONCNOs composite has a nearly ideal rectangular shape with a specific capacitance of 43 $F•g^{-1}$. A cycling study over 1000 cycles at 2.0 $A•g^{-1}$ for the PDDA/ONCNOs showed the retention of ~84% of initial capaciatance. Cyclic voltammetry studies of composites containing varying concentrations of MnO_2 are plotted in **Fig. 5.2**. With increasing MnO_2 concentration, capacitance increases linearly with a maximum value of 218.6 $F•g^{-1}$ for the 55 wt % MnO_2 composite electrode.

To compare the performance of composites with different wt % of MnO_2, a scan rate of 5 mV/s is used. As the scan rate increases, the capacitance drops rapidly (**Fig. S2** in the supplimentary information). A thin, single layer of delaminated MnO_2 on conductive carbon is expected to overcome the inherent low conductivity of MnO_2 layers. However, as observed from the HRTEM (**Fig. 4**), MnO_2 layers re-aggregate upon drying, which lowers the conductivity and increases the ESR of the resultant materials. This is also reflected in the CV plots (**Fig. 5.1**) and the impedance spectra (**Fig. 5.2**) of the composites, which become more resistive with increasing MnO_2 concentration. Moreover, after the electrochemical measurements a thin brown ring on the Celgard separator is observed, which is due to the partial dissolution of MnO_2. At typical applied polarization potentials, MnO_2 is irreversibly oxidized to soluble Mn(VII) at the positive electrode and irreducibly reduced to soluble Mn(II) at the negative electrode in neutral electrolyte.[25] Thus, above the limiting potential window of MnO_2 in aqueous electrolyte, the irreversible redox reactions will eventually destabilize the material. We suggest that

the interaction of the positively charged PDDA/ONCNOs surface with the negatively charged MnO_2 layers stabilizes the ternary composite. In the MnO_2/PDDA/ONCNOs composites, the re-aggregated MnO_2 nano-sheets have weaker interaction with the positively charged PDDA/ONCNOs surface. As the number of MnO_2 layers increases, the materials became more resistive; as observed from the ESR of the impedance study (**Fig. 5.4**). At lower concentrations of MnO_2, when the re-aggregation is limited, the materials exhibit low capacitance due to a smaller number of redox sites of MnO_2 but no noticeable brown spots were observed on the Celgard separator after charge-discharge cycling. At very high concentration of MnO_2, the outermost MnO_2 layers that are loosely interacting with the positively charged PDDA/ONCNOs are most likely to dissolve under repeated charge-discharge conditions producing prominent brown spots. As a result the concentration of MnO_2 on composites was optimized to 55 wt% . Thus, we found that high capacitance and better stability could be achieved by adjusting the ratio between MnO_2 and PDDA/ONCNOs and by sequential deposition of the components to creat a positive synergistic effect in the composite electrodes. Interestingly, during cycling study the positively charged PDDA/ONCNOs materials show intial increase in capacitance followed by slow decrease to a steady state, while MnO_2/PDDA/ONCNOs composites show usual behavior of initial decrease in capacitance followed by a nearly stable value. The differences in surface chemistry of the materials influence the cyclic behavior of the PDDA/ONCNOs and MnO_2/PDDA/ONCNOs. While Faradic reactions were originated from the polyelectrolyte (PDDA) covered surface of ONCNOs for PDDA/ONCNOs, it is the MnO_2 redox sites that contribute to the pseudocapacitance of MnO_2/PDDA/ONCNOs composites. Also, the swelling of polyelectrolytes under charge-discharge cycling

influences the establishment of initial electrochemical equilibrium. Charge-discharge cycling study of PDDA/ONCNOs and MnO_2/PDDA/ONCNOs composite show retention of ~84% and ~81% of intial capacitance respectively (**Fig. 6**).
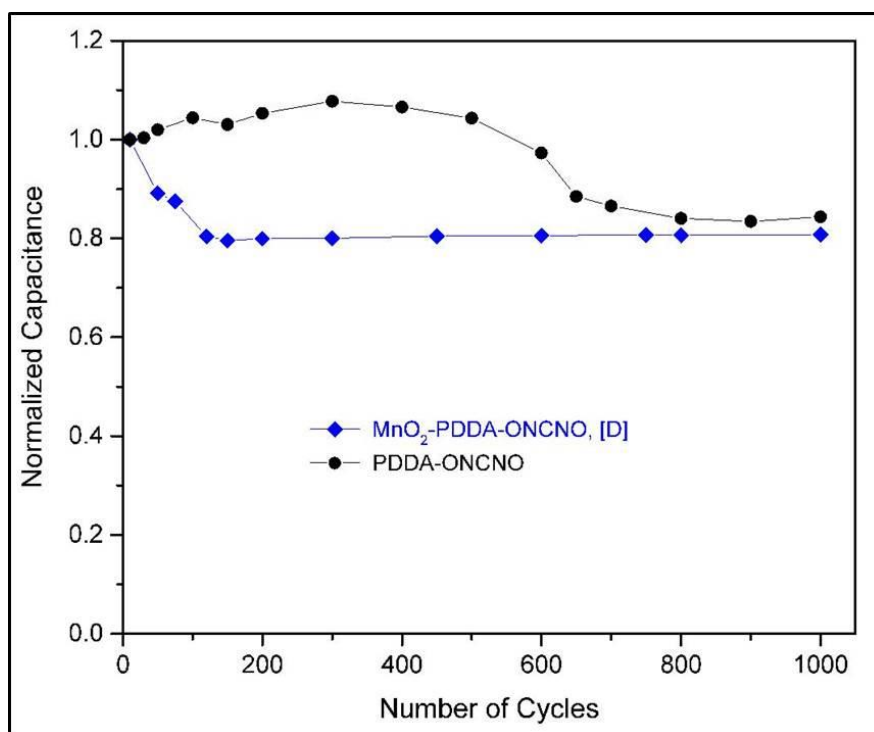
Figure 6. Charge-discharge cycling stability of PDDA/ONCNOs and MnO_2 (44.0 wt %) /PDDA/ONCNOs [D].

This synthesis approach has the advantage over a more common approach of depositing a stable layer on top of MnO_2, because the stable layer could limit the accessibility of the electrolytic ions into the buried redox active sites of MnO_2. However, future research is necessary to fully explore the synergetic effects of the MnO_2-based composite electrodes to mitigate their low conductivity and low cycling stability for a broader potential window in aqueous electrolytes.

5. Conclusions:

17

We have successfully synthesized MnO_2/PDDA/ONCNOs composites using the unique properties of NCNOs, thin layer of PDDA, and delaminated MnO_2 to achieve high-capacitance. Sequential deposition is a simple and effective technique to synthesize ternary composites for MnO_2-based electrodes. This work demonstrates the importance of sequential deposition and step-by-step tuning of the materials' surface chemistry for overall positive synergistic effect, enabling higher capacitance and electrochemical stability of MnO_2-based composites for supercapacitor electrodes. Also, the unique tunable surface properties of carbon nano-onions for chemical synthesis of composite electrodes were highlighted.

We believe this work, which demonstrates a potentially low-cost synthetic method, application of carbon nano-onions and an approach to utilize synergistic properties of charged layer structures will stimulate future research on high performance MnO_2-carbon composite materials for supercapacitor applications.

18

References:

1.   H.I. Becker, in: G. Electrics (Ed.), *US Pat.,* 1957.
2.   W. Wei, X. Cui, W. Chen and D. G. Ivey, *Chem. Soc. Rev.*, 2011, 40, 1697-1721.
3.   X. Liu, C. Chen, Y. Zhao and B. Jia, *J. Nanomater.*, 2013, 2013, 7.
4.   E. Raymundo-Pinero, V. Khomenko, E. Frackowiak and F. Beguin, *J. Electrochem. Soc.*, 2005, 152, A229-A235.
5.   H. The An, T. Van Man and L. My Loan Phung, *Adv. Nat. Sci: Nanosci. Nanotechnol.*, 2013, 4, 035004.
6.   A. E. Fischer, K. A. Pettigrew, D. R. Rolison, R. M. Stroud and J. W. Long, *Nano Lett.*, 2007, 7, 281-286.
7.   J. Liu, J. Essner and J. Li, *Chem. Mater.*, 2010, 22, 5022-5030.
8.   S. Hassan, M. Suzuki, S. Mori and A. A. El-Moneim, *J. Power Sources*, 2014, 249, 21-27.
9.   X. Zhao, L. Zhang, S. Murali, M. D. Stoller, Q. Zhang, Y. Zhu and R. S. Ruoff, *ACS Nano*, 2012, 6, 5404-5412.
10.   R. Jiang, C. Cui and H. Ma, *Electrochim. Acta*, 2013, 104, 198-207.
11.   S. R. Sivakkumar, J. M. Ko, D. Y. Kim, B. C. Kim and G. G. Wallace, *Electrochim. Acta*, 2007, 52, 7377-7385.
12.   M. Toupin, T. Brousse and D. Bélanger, *Chem. Mater.*, 2002, 14, 3946-3952.
13.   P. Lv, P. Zhang, Y. Feng, Y. Li and W. Feng, *Electrochim. Acta*, 2012, 78, 515-523.
14.   C.-C. Wang, H.-C. Chen and S.-Y. Lu, *Chem. Eur. J.*, 2014, 20, 517-523.
15.   Y. Wang, S. F. Yu, C. Y. Sun, T. J. Zhu and H. Y. Yang, *J. Mater. Chem.*, 2012, 22, 17584-17588.
16.   R. Borgohain, J. Li, J. P. Selegue and Y. T. Cheng, *J. Phys. Chem. C*, 2012, 116, 15068-15075.
17.   M. E. Plonska-Brzezinska and L. Echegoyen, *J. Mater. Chem. A*, 2013, 1, 13703-13714.
18.   R. Borgohain, J. Yang, J. P. Selegue and D. Y. Kim, *Carbon*, 2014, 66, 272-284.
19.   S. Park, K. Lian and Y. Gogotsi, *J. Electrochem. Soc.*, 2009, 156, A921-A926.
20.   M. E. Plonska-Brzezinska, A. Palkar, K. Winkler and L. Echegoyen, *Electrochem. Solid-State Lett.*, 2010, 13, K35.
21.   D. Pech, M. Brunet, H. Durou, P. Huang, V. Mochalin, Y. Gogotsi, P.-L. Taberna and P. Simon, *Nat Nano*, 2010, 5, 651-654.
22.   Y. Ma, J. Luo and S. L. Suib, *Chem. Mater.*, 1999, 11, 1972-1979.
23.   Q. Gao, O. Giraldo, W. Tong and S. L. Suib, *Chem. Mater.*, 2001, 13, 778-786.
24.   Z.-h. Liu, K. Ooi, H. Kanoh, W.-p. Tang and T. Tomida, *Langmuir*, 2000, 16, 4154-4164.
25.   V. Khomenko, E. Raymundo-Piñero and F. Béguin, *J. Power Sources*, 2006, 153, 183-190.
26.   S. Wang, D. Yu and L. Dai, *J. Am. Chem. Soc.*, 2011, 133, 5182-5185.